Environmental Science & Technology

Article

pubs.acs.org/est

Spatial Distribution and Speciation of Arsenic in Peat Studied with Microfocused X-ray Fluorescence Spectrometry and X-ray Absorption Spectroscopy

Peggy Langner,[†] Christian Mikutta,*[,†] Elke Suess,[†] Matthew A. Marcus,[‡] and Ruben Kretzschmar[†]

[†]Institute of Biogeochemistry and Pollutant Dynamics, Department of Environmental Systems Science, ETH Zurich, 8092 Zurich, Switzerland

[‡]Advanced Light Source, Lawrence Berkeley National Laboratory, 1 Cyclotron Road, Berkeley, California 94720, United States

Supporting Information

ABSTRACT: Arsenic binding by sulfhydryl groups of natural organic matter (NOM) was recently identified as an important As sequestration pathway in the naturally As-enriched minerotrophic peatland *Gola di Lago*, Switzerland. Here, we explore the microscale distribution, elemental correlations, and chemical speciation of As in the *Gola di Lago* peat. Thin sections of undisturbed peat samples from 0−37 cm and 200−249 cm depth were analyzed by synchrotron microfocused X-ray fluorescence (μ-XRF) spectrometry and X-ray absorption spectroscopy (μ-XAS). Additionally, peat samples were studied by bulk As, Fe, and S *K*-edge XAS. Micro-XRF analyses showed that As in the near-surface peat was mainly concentrated in 10−50 μm sized hotspots, identified by μ-XAS as realgar (α-As_4S_4). In the deep peat layer samples, however, As was more diffusely distributed and mostly associated with particulate NOM of varying decomposition stages. The NOM-associated As was present as trivalent As bound by sulfhydryl groups. Arsenopyrite (FeAsS) and arsenian pyrite ($FeAs_xS_{2-x}$) of <25 μm size, which have escaped detection by bulk As and Fe *K*-edge XAS, were found as minor As species in the peat. Bulk S *K*-edge XAS revealed that the deep peat layers were significantly enriched in reduced organic S species. Our findings suggest an authigenic formation of realgar and arsenopyrite in strongly reducing microenvironments of the peat and indicate that As(III)−NOM complexes are formed by the passive sorption of As(III) to NOM. This reaction appears to be favored by a combination of abundant reduced organic S and comparatively low As solution concentrations preventing the formation of secondary As-bearing sulfides.

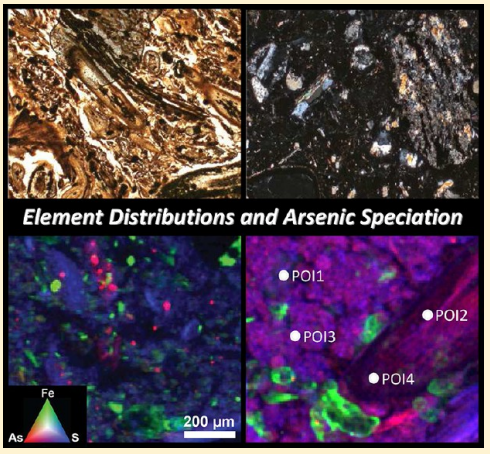

INTRODUCTION

Wetland soils are sensitive ecosystems that play an important role in the storage, transformation, and mobilization of nutrients and contaminants. Besides natural sources, anthropogenic emissions from mining and smelting, fossil fuel combustion and agriculture have led to the accumulation of toxic trace elements like As in a number of wetland soils and peaty sediments which may pose a continuing risk for surface and groundwater quality as well as ecosystem health.[1−4]

Arsenic is a redox-sensitive element whose toxicity and fate in the environment strongly depends on its oxidation state and speciation.[5] Inorganic As commonly comprises arsenate, As(V), in oxic, and the more toxic arsenite, As(III), in anoxic environments low in S.[5] In aerated soils and sediments, As(V) has a strong affinity toward mineral surfaces, rendering it comparatively immobile.[5−8] In O_2 depleted soils and sediments, microbial decomposition of natural organic matter (NOM) drives the reductive dissolution of metal-(hydr)oxides and thus the release of associated As(V) and its redox transformation into As(III).[9,10] The released As(III) may subsequently be immobilized by Fe sulfides[11,12] or mixed valence metal-(hydr)oxides,[13,14] or precipitate as As sulfide.[2,15,16] In addition, several studies provided indirect evidence for an association of As with NOM under reducing conditions,[1,9,17−19] but spectroscopic assessments of the governing binding mechanisms and their environmental relevance are still scarce. In a recent bulk X-ray absorption spectroscopy (XAS) study on the solid-phase speciation of As in a naturally As-enriched (≤1800 mg As kg^{-1}), slightly acidic minerotrophic peatland (*Gola di Lago*, Switzerland), we observed that in deep peat layers (150−250 cm) As was predominantly sequestered by NOM in its trivalent oxidation state ("As(III)−NOM complexes"). Shell-fit analyses of As *K*-edge extended X-ray absorption fine structure (EXAFS) spectra of these samples revealed S coordination numbers of 2−3 and interatomic As−S distances of 2.26 Å,

Received: March 25, 2013
Revised: July 18, 2013
Accepted: July 26, 2013
Published: July 26, 2013

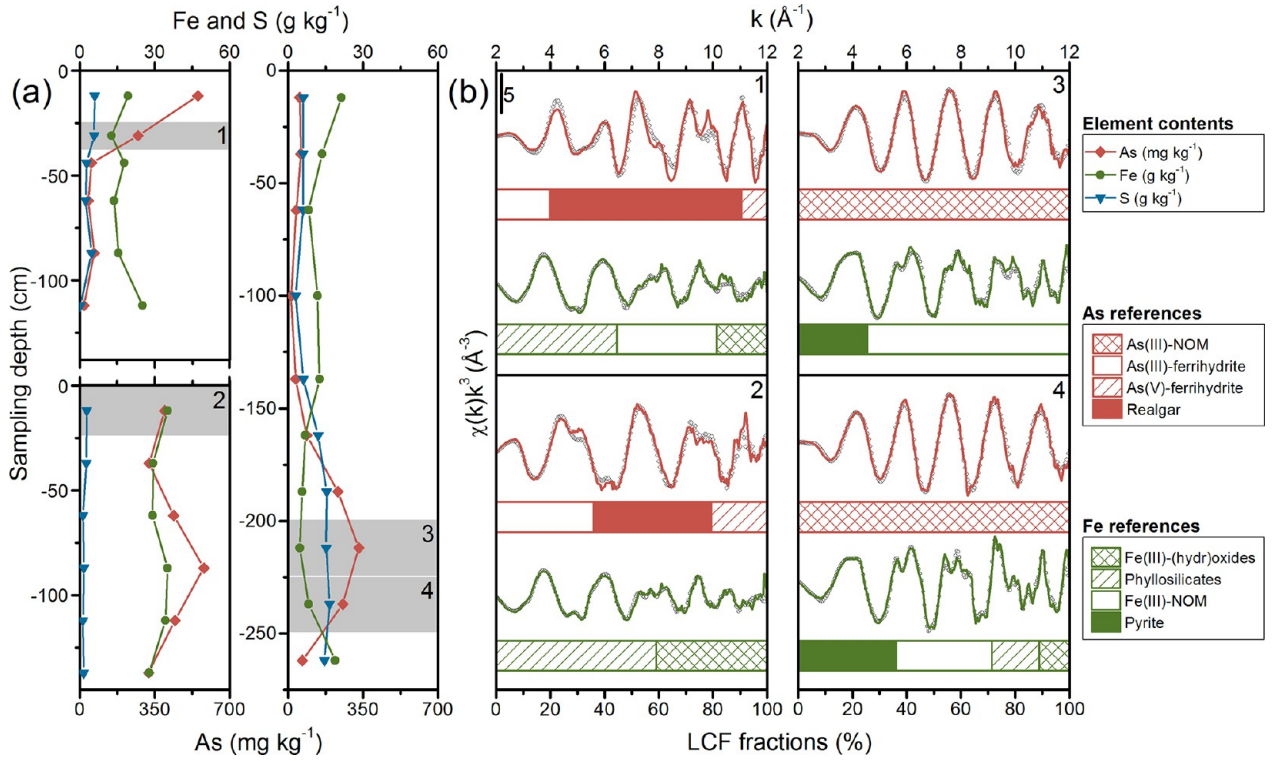

Figure 1. (a) Distribution of As, Fe, and S in peat cores B3II (top left), B5II (bottom left), and B1II (right). Concentrations are given on a dry-weight basis. Gray-shaded boxes (1−4) indicate the depth intervals from which samples were taken for bulk and microspectroscopic analyses. (b) Bulk As and Fe *K*-edge EXAFS spectra (lines) and corresponding best model fits (symbols) are shown for each depth interval with the As *K*-edge EXAFS plotted on top of the respective Fe *K*-edge EXAFS. The numbers in the upper right corner of each box correspond with those in the gray-shaded boxes in (a). The horizontal bars display the percent fraction of each reference compound fitted in the LCF analysis. The concentrations of As, Fe, and S are summarized in Table S1, Supporting Information, and the bulk speciation results for As and Fe are reported in Tables S2 and S3, Supporting Information.

values typical of inner-sphere As(III) complexes with sulfhydryl groups.[20] In contrast to the deep peat layers, near-surface peat samples (0−41 cm) showed a variety of As species, including realgar (α-As_4S_4), As(III/V) sorbed to Fe(III)-(hydr)oxides, and As(III)−NOM complexes. These two contrasting As speciation patterns suggest fundamental differences in the distribution of As within the peat. While bulk As *K*-edge XAS analyses yield information about the average coordination environment of As, they do not provide information on its spatial distribution, elemental correlations, and chemical speciation at the microscale. Bulk XAS analyses may also fail to detect minor As species having a potentially high geochemical activity. Here, we employed microfocused X-ray fluorescence (μ-XRF) spectrometry in combination with microfocused XAS (μ-XAS) to investigate the spatial distribution, elemental correlations, and speciation of As in the *Gola di Lago* peatland. These techniques have previously been used to investigate the distribution and to some extent the speciation of As in plant roots as well as As-rich soils and sediments.[12,21−25] Hitherto, spatially resolved information on As distribution and speciation in NOM-dominated soils and sediments subject to permanent or periodic water-logging is currently not available but may provide new insights into geochemical conditions favoring particular As sequestration pathways.

The overall goal of this study was thus to provide the first information on the microscale distribution and speciation of As in a NOM-rich soil environment characterized by substantial differences in As speciation. More specifically, we used μ-XRF spectrometry and μ-XAS (i) to investigate the size and distribution of As sulfide minerals in the uppermost peat layers of the *Gola di Lago* site, (ii) to assess the distribution pattern of As(III)−NOM complexes in the deep peat layers, and (iii) to identify minor As species.

MATERIALS AND METHODS

Field Site and Sampling. In a preceding study, we sampled peat cores at locations B1−8 close to an As-rich intermittent stream of the minerotrophic peatland *Gola di Lago* (canton Ticino, Switzerland) and analyzed the solid-phase speciation of As and Fe by bulk XAS.[20] In September 2009, we collected two additional peat cores less than 25 cm away from each of the initial sampling locations B1, B3, and B5.[20] These two peat cores are labeled "I" and "II" in the following. Undisturbed peat material was sampled in ∼25 cm intervals using Kubiena boxes made of bladed Al (8 cm × 6 cm × 5 cm). The boxes and all samples used for bulk speciation measurements of S were instantly shock-frozen in liquid N_2, transported on dry ice to the laboratory, and processed in an anoxic glovebox (O_2 <10 ppm). Additional material of each peat sample was used for general sample characterization as described in ref 20. Redox potential, pH, and electrical conductivity of the field-moist, mostly water-saturated peat samples were immediately measured on-site.

Sample Preparation and Synchrotron Measurements. On the basis of the elemental composition and previous results from bulk As and Fe XAS analyses,[20] four samples were selected for the preparation of thin sections as well as for bulk

dx.doi.org/10.1021/es401315e | Environ. Sci. Technol. 2013, 47, 9706−9714

XAS and synchrotron X-ray diffraction (SXRD) measurements from peat cores B1II (200−224 and 225−249 cm), B3II (25−37 cm), and B5II (0−24 cm) (Figure 1). For the sake of clarity, the sample notation will be confined to core label and mean sampling depth in centimeters, for example, B1II-212 or B3II-31. The four Kubiena boxes were freeze-dried and immediately transferred in Ar atmosphere into an anoxic glovebox, where they were impregnated with epoxy resin (Epotek 301-2FL, Epoxy Technology Inc., USA). Sections of 1 mm thickness were then cut using a diamond saw, mounted on As-free silica glass slides, and polished down to a thickness of 30 μm under exclusion of O_2 (Spectrum Petrographics Inc., USA). A subsample of each Kubiena box was prepared for bulk As and Fe XAS and SXRD analyses. The sample preparation for XAS analyses was identical to that described in ref 20. For SXRD measurements, homogenized peat material was filled into 1 mm o.d. borosilicate glass capillaries. Peat samples used for S *K*-edge XAS analysis were prepared in the same manner as those used for As and Fe XAS analyses, except that the samples were diluted to a concentration of 1800 mg S kg^{-1} using BN in order to reduce overabsorption effects[26] and pressed into 1.3 cm pellets.

Bulk As *K*-edge (11867 eV), Fe *K*-edge (7112 eV), and S *K*-edge (2472 eV) XAS spectra were collected in fluorescence mode at beamlines 11−2 (As), 4−1 (Fe), and 4−3 (S) of the Stanford Synchrotron Radiation Lightsource (SSRL, SLAC National Accelerator Laboratory, Menlo Park, USA). The thin sections were analyzed by μ-XRF spectrometry and μ-XAS at beamline 10.3.2 of the Advanced Light Source (ALS, Berkeley, USA) after identification of representative regions using plane- and cross-polarized light microscopy (Zeiss Axioskop 40 microscope). The mineralogy of the peat samples was investigated by SXRD. These measurements were conducted at the powder diffraction station of the Material Sciences (MS-Powder) beamline at the Swiss Light Source (SLS, Villingen, Switzerland). Details about all experimental setups, measurement conditions, and data evaluations can be found in the Supporting Information.

RESULTS

Peat Characterization. For the investigation of the microscale distribution and speciation of As in the *Gola di Lago* peatland, three sampling locations characterized by two different As speciation patterns were selected. At locations B3 and B5, As was enriched in the top 41 cm and mainly present as realgar and As(III/V) sorbed to Fe(III)-(hydr)oxides. At location B1, however, As was concentrated at 150−200 cm depth and entirely sequestered as trivalent As by organic S.[20] The field-moist peat sampled in September 2009 and used for this study (cores B1I/II, B3I/II, and B5I/II) was slightly acidic (pH 5.7 ± 0.5). The redox potential, E_h, ranged from −11 to 364 mV, and the mean ionic strength estimated from electrical conductivity values[27] was 9×10^{-4} *M* (n = 54). Arsenic, Fe, and S concentrations in the "II" peat cores are displayed in Figure 1 and summarized together with those of other major elements in Table S1, Supporting Information. Except for core B5II, the As-enriched zones in peat cores B1II (175−249 cm) and B3II (0−37 cm) were located at approximately the same depths as those of the initial peat cores B1 and B3 collected in March 2009.[20] The concentration maxima of As in the "II" peat cores (331−580 mg As kg^{-1}), however, were up to five times lower compared to the initial peat cores (469−1800 mg As kg^{-1}), emphasizing the high spatial variability of As at the decimeter scale.

Synchrotron XRD patterns of peat samples used for μ-XRF and μ-XAS analyses (Figure 1), which are displayed in Figure S1, Supporting Information, confirmed the presence of primary minerals in the near-surface peat samples B3II-31 and B5II-12, including quartz, phyllosilicates (biotite, muscovite, chlorite), and plagioclase (albite, oligoclase, anorthite). The deep peat layer samples of core B1II showed Bragg peaks belonging to quartz, muscovite, plagioclase (albite, oligoclase), and pyrite. Mineral-phase assemblages in the thin sections studied by μ-XRF spectrometry and μ-XAS were also investigated by light microscopy. These analyses revealed considerable amounts of mineral phases embedded in the organic matrix of the near-surface peat sample B3II-31, which included single particles (∼100−500 μm) of plagioclase, quartz, mica-group minerals (biotite, muscovite), some epidote, and chlorite, as well as altered rock fragments of mainly gneiss (∼1−3 mm) (Figure S2, Supporting Information). In contrast, mineral phases were less abundant in the two thin sections of the deep peat layer samples B1II-212 and B1II-237, and only comprised quartz and mica particles (∼10−50 μm) (Figures S2 and S3, Supporting Information). Using cross-polarized light,[28] however, we detected fine-grained, reddish-brown colored secondary Fe-(hydr)oxides in all thin sections, partially infilling pores or coating mineral surfaces (Figure S3, Supporting Information).

Bulk XAS Analyses. Bulk As and Fe *K*-edge EXAFS spectra of all four peat samples used to prepare the thin sections are illustrated in Figure 1 along with the corresponding linear combination fits (LCF). The LCF results for As and Fe, shown as horizontal bars in Figure 1, are compiled in Tables S2 and S3, Supporting Information. In the near-surface peat layer samples B3II-31 and B5II-12, the major As species comprised realgar (43−71%) and As(III) (20−36%) as well as As(V) (9−21%) sorbed to Fe(III)-(hydr)oxides. In contrast, As(III)−NOM complexes completely dominated the As speciation in the deep-peat layer samples B1II-212 and B1II-237, in agreement with our earlier findings.[20] The presence of pararealgar, a polymorph of realgar, in the near-surface peat samples can be excluded since its local As coordination (e.g., r_{As-As} = 2.48−2.53 vs. 2.57 Å)[29−31] and hence As *K*-edge EXAFS differs from that of realgar (not shown). Other modifications of realgar (β-As_4S_4 and As_4S_4(II)) can also be dismissed since they do not form in low pressure/low temperature environments.[31−33] Note also that orpiment (As_2S_3) was not detected in any peat sample.

The LCF results of the bulk Fe *K*-edge EXAFS spectra revealed that the major Fe species in the near-surface peat layer samples included Fe(III)-(hydr)oxides (19−41%), phyllosilicates (44−59%), and Fe(III)−NOM complexes (0−37%). Iron in the deep peat layer samples was predominantly present as Fe(III)−NOM complexes (35−75%) and pyrite (25−36%), whereas Fe(III)-(hydr)oxides (0−11%) and phyllosilicates (0−18%) were much less abundant (Figure 1, Table S3, Supporting Information). These findings are in general agreement with our SXRD, light microscopy, and As speciation results (Figures S1−3 and Table S2, Supporting Information).

The differences in As and Fe speciation observed for the near-surface and deep peat layer samples (Figure 1) suggest important differences in the bulk S speciation as a function of depth. For this reason, we also studied the speciation of S in peat material originating from peat cores B1I, B3I, and B5I. These samples were taken from similar depths as those of the

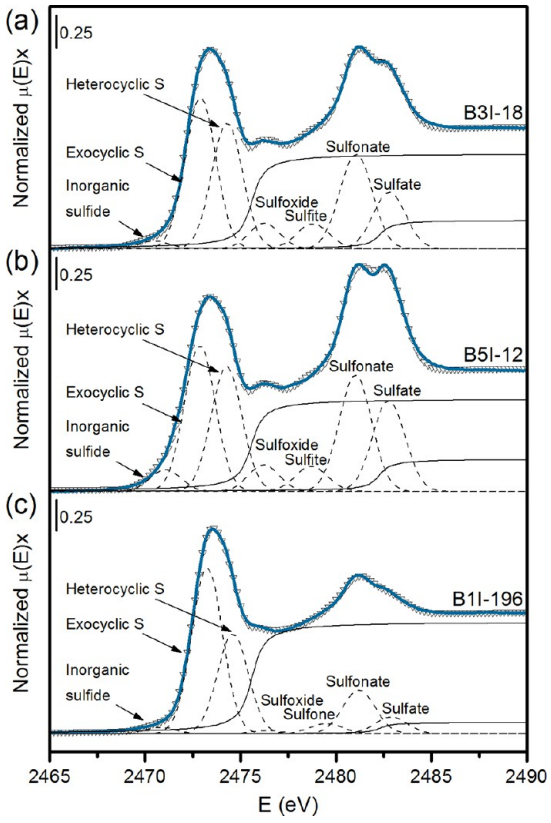

Figure 2. Deconvolution of normalized bulk S *K*-edge XANES spectra into several Gaussians and two arctangent curves of the near-surface peat samples (a) B3I-18 and (b) B5I-12, as well as the deep peat layer sample (c) B1I-196. Data is shown as solid blue lines, fit envelopes as symbols, fit components as dashed lines, and arctangent functions as solid black lines. Parameter values and fit results are summarized in Tables S4 and S5, Supporting Information.

"II" peat cores and also had similar S contents (Table S4, Supporting Information). Figure 2 shows the S *K*-edge XANES spectra of peat samples B3I-18, B5I-12, and B1I-196, as well as their spectral deconvolution based on Gaussians representing resonance peaks of the main S functionalities.[34] All peat samples showed two distinct resonance-peak ranges. The first peak range from 2471 to 2475 eV includes "reduced S" species (inorganic sulfide and organic exocyclic/heterocyclic S), and the second peak ranging from 2481 to 2483 eV represents "oxidized S" species (sulfonate and sulfate). "Intermediate oxidized S" species (sulfoxide, sulfite, and sulfone) with resonance peaks located between 2476 and 2480 eV were generally of less quantitative importance (Tables S4 and S5, Supporting Information).

Both "oxidized" and "intermediate oxidized" S species were more abundant in the near-surface peat samples B3I-18 and B5I-12 compared to the deep peat layer sample B1I-196 (Figure 2, Table S4, Supporting Information). However, the fitted fractions of sulfoxide, sulfite, and sulfone S as part of the "intermediate oxidized S" are presumably overestimated in all samples, since the energy range of 2476−2480 eV is significantly affected by postedge absorption features of reduced organic S species as well as the first arctangent function.[35] Due to their low quantitative importance and in order to obtain a generally reasonable fit quality, these "intermediate oxidized S" species were nonetheless included in our fitting procedure.

With 80−92% of total S, "reduced S" was the dominant S form in all peat samples (Table S4, Supporting Information). Inorganic sulfide S only comprised 9−16% of the "reduced S" pool. A significant attenuation of the inorganic sulfide signal due to the limited X-ray penetration depth at the S *K*-edge[36] can be ruled out because the pyrites observed in the *Gola di Lago* peat were smaller than one absorption length calculated for pyrite at 2.5 keV.[20] Thus, according to the white-line positions,[34,35,37] the majority of S can be attributed to reduced organic S species (64−83%), which falls at the high end of reduced organic S in peatlands (14−87%).[35,38−42] Even though the relative amount of reduced organic S in the near-surface and deep peat layer samples was comparable, the deep peat layer sample contained 2−7 times more S. Thus, its reduced organic S pool significantly exceeded that of the shallow peat layer samples.

μ-XRF and μ-XAS Analyses. Elemental mapping by μ-XRF spectrometry was employed to investigate the distribution of As and its correlations with other elements, notably Fe and S. On the basis of the elemental associations of As, μ-XAS analysis was used to identify major and minor As species at selected points of interest (POIs). Figure 3 shows coarse and fine elemental distribution maps of As, Fe, and S obtained from thin sections of the near-surface peat layer sample B3II-31 and the deep peat layer sample B1II-237. The distributions of As and Fe in the near-surface peat sample B5II-12 and the second deep peat layer sample B1II-212 are additionally depicted in Figure 4. The elemental distribution maps document that the distribution of As in the near-surface peat samples differed substantially from that in the deep peat layer samples. Whereas intense As hotspots of about 10−50 μm size dominated the near-surface peat samples, As was for the most part more diffusely distributed in the deep peat layer samples and associated with plant fibers (Figure 3) and brownish NOM with a "cauliflower"-like morphology representing more humified NOM (Figure 4b, Figure S3d−f, Supporting Information). At the As hotspots found mostly close to the peat surface, a clear correlation with S was recognized (Figure S4a−c, Supporting Information). A second As−S correlation, characterized by lower As/S ratios, was additionally noticed in the near-surface peat sample B3II-31 and was linked to the diffuse As distribution in this particular sample (Figure S4d−f, Supporting Information). For the deep peat layer thin sections, we also observed two pronounced correlations between As and S. Whereas the first correlation corresponds to the diffuse distribution of As, the second is restricted to rare but intense As hotspots (Figure S4g−l, Supporting Information).

Correlations between As and Fe ranged from strong to nonexistent (Figure S5, Supporting Information). The most evident As−Fe correlation was found in a deep peat layer sample, where Fe-rich As hotspots were particularly enriched in S, pointing toward arsenopyrite and/or arsenian pyrite (Figure S4g−i vs. Figure S5g−i, Supporting Information). In contrast, Fe correlated well with Mn in all samples, particularly in the near-surface peat samples (Figure S6, Supporting Information). Here, a significant portion of Fe and Mn was associated with Si-poor secondary Fe-(hydr)oxides identified by light microscopy (Figures S3 and S7, Supporting Information).

The speciation of As was studied by As *K*-edge μ-XAS at selected POIs indicated in each fine map shown in Figures 3 and 4. Similar POI spectra were averaged in order to increase the signal-to-noise ratio. The μ-XANES spectra and their LCFs are illustrated in Figure 5 along with the k^2-weighted μ-EXAFS

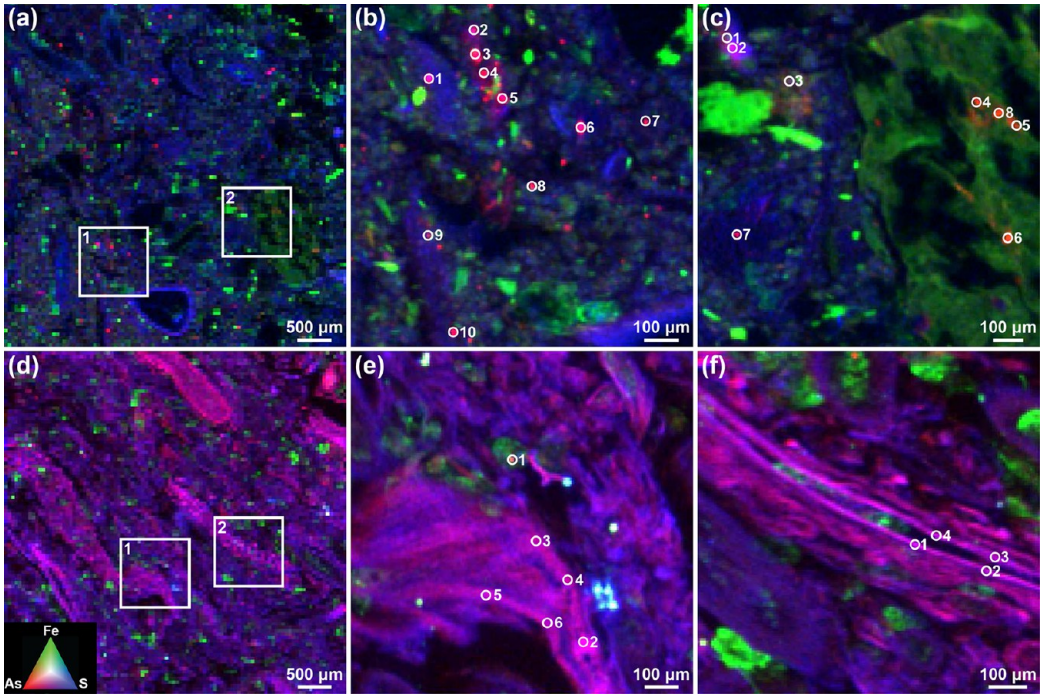

Figure 3. Tricolor (RGB) μ-XRF maps of the distribution of As, Fe, and S in thin sections of (a–c) the near-surface peat layer sample B3II-31 and (d–f) the deep peat layer sample B1II-237. (a, d) Overview maps indicating the location of regions 1 and 2 in each thin section. (b, e) Fine maps of regions 1, and (c, f) fine maps of regions 2. The points of interest (POIs) selected for μ-XAS analysis are shown in each fine map. The color code in (d) is valid for all panels.

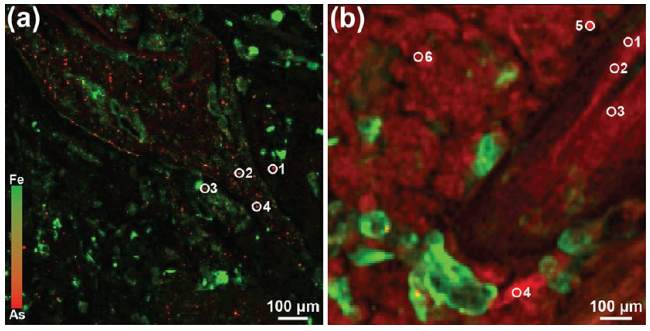

Figure 4. Bicolor (RG) μ-XRF map of the As and Fe distribution in thin sections of (a) the near-surface peat layer sample B5II-12 and (b) the deep peat layer sample B1II-212. The points of interest (POIs) selected for μ-XAS analysis are also shown in each map. The color code in (a) is valid for both panels.

spectra and their spectral reconstructions based on the LCF results, which are summarized in Table 1. All analyzed As hotspots in region 1 of the B3II-31 thin section (Figure 3b) entirely consisted of realgar. The POIs of region 2 of the B3II-31 sample (Figure 3c) were well fitted with variable mixtures of realgar (0–84%), As(III)–NOM complexes (0–44%), and As(III) (16–44%) as well as As(V) (0–71%) sorbed to Fe(III)-(hydr)oxides (Table 1). Interestingly, all POIs (4–6, 8) located on the highly altered gneiss fragment in the region 2 map (Figure 3c, Figure S2, Supporting Information) were dominated by As(III/V) sorbed to Fe(III)-(hydr)oxides, which are most likely weathering products of Fe-bearing silicates.

Realgar was not the only As mineral detected in the near-surface peat samples. Figure 4 shows ~10 μm sized As hotspots partially strung along plant fibers in the B5I-12 sample. Micro-XAS analysis of these spots confirmed the presence of arsenopyrite (FeAsS) (Table 1).

Arsenic *K*-edge μ-XAS analysis of the deep peat layer thin sections of core B1II revealed that trivalent As coordinated to sulfhydryl groups of NOM (Table 1) constitutes the diffusely distributed As found either on fibrous plant remains or on more humified NOM (Figure 3e,f vs. Figure 4b, Figures S2 and S3, Supporting Information). Besides As(III)–NOM complexes as dominating As species, several hotspots enriched in As, Fe, and S with an approximate size of less than 25 μm were readily discernible in the deep peat layer samples (Figure 3e). While the whitish spots (rich in As, Fe, and S) indicate the presence of arsenopyrite, the As μ-XAS spectrum collected at POI1 (Figure 3e) confirmed a mixture of 35% arsenopyrite and 65% arsenian pyrite (Table 1). Neither of these minerals was accepted as reference compound in LCF analyses of bulk As and Fe EXAFS spectra, implying that they were only present in trace amounts.

DISCUSSION

The bulk As speciation results (Figure 1) in conjunction with absent As–Fe correlations related to Fe(III)-(hydr)oxides (Figure S5, Supporting Information) show that these phases are of minor importance for the immobilization of As at the study site, despite that they typically play a crucial role in As sequestration.[5,8] Nonetheless, because they comprise up to 41% of total Fe, they can be expected to be effective scavengers of As released upon As sulfide oxidation following a seasonal drop in the water table.

Our μ-XRF and μ-XAS analyses also document that the two distinct As enrichment patterns observed in the *Gola di Lago* peatland[20] are linked to two contrasting microscale As speciation and distribution patterns. Where As solution concentrations are high ($\leq$5.4 μM) as in the surface waters entering the peatland,[19] they favor the precipitation of

dx.doi.org/10.1021/es401315e | Environ. Sci. Technol. 2013, 47, 9706–9714

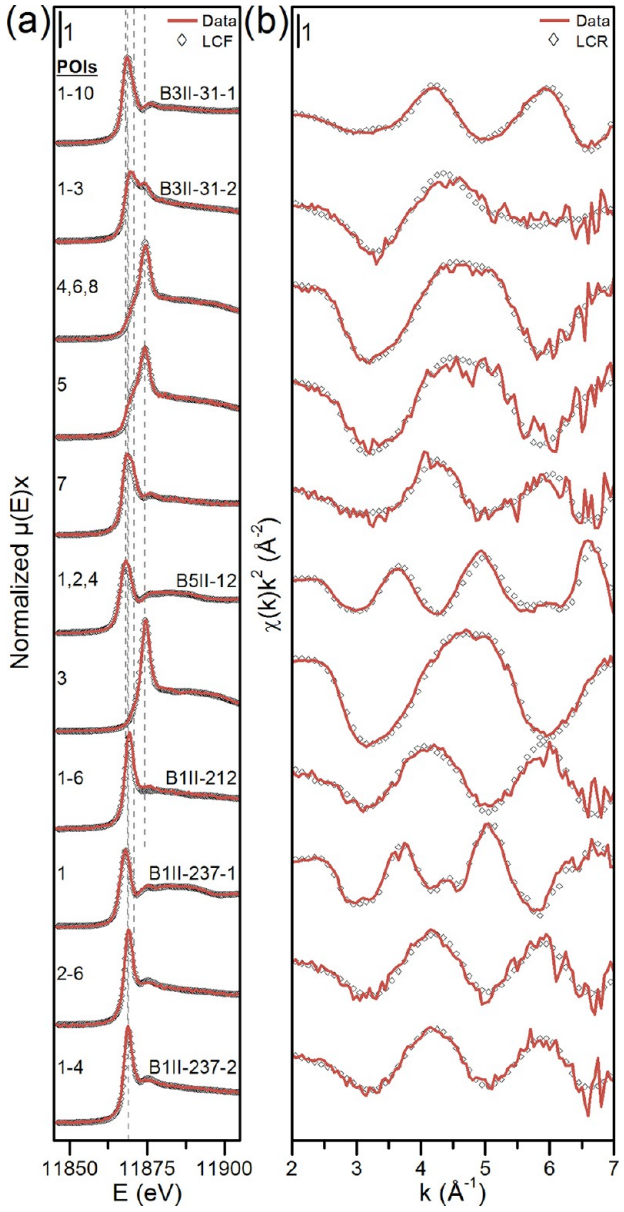

Figure 5. (a) Normalized As *K*-edge μ-XANES and (b) k^2-weighted μ-EXAFS spectra averaging selected POIs of thin sections from peat cores B1II, B3II, and B5II (Figures 3 and 4). The sample notation indicates core number, mean sampling depth of the thin section material in centimeters, and (where applicable) the number of the mapped region. Experimental data is shown as solid lines, and symbols represent linear combination fits (LCF) of the μ-XANES spectra and linear combination reconstructions (LCR) of the μ-EXAFS spectra based on the LCF results. LCF was performed from −15 to 20 eV ($E-E_0$). The vertical lines in (a) indicate white-line positions of As(-I), As(II), As(III), and As(V) reference compounds (from left to right). The fit results are reported in Table 1.

micrometer-sized (10−50 μm) As sulfides in shallow peat layers close to the stream inflow. The in-situ formation of realgar in low-temperature/low pressure environments has so far only been observed in a shallow aquifer sediment.[43] Reaction path modeling indicated that realgar precipitation is favored in anoxic circum-neutral pH environments, where the H_2S activity is buffered by the coexistence of Fe sulfides and Fe(II/III)-(hydr)oxides.[43] Under such conditions, As(III) can be reduced by Fe monosulfides, leading to the formation of realgar and greigite (Fe_3S_4):[44,45]

$$3FeS + H_3AsO_3 + 3H^+ \leftrightarrow 1/2Fe_3S_4 + AsS + 3/2Fe^{2+} + 3H_2O \quad \Delta G^0 = -88.6\ kJ\ mol^{-1} \quad (1)$$

The Gibbs free energy change of reaction was calculated for mackinawite (FeS), and all thermodynamic data used for this and all subsequent reaction equations are tabulated in Table S6, Supporting Information. Despite that eq 1 is thermodynamically favorable, we did not detect any Fe sulfide phase in the shallow peat layers by bulk Fe *K*-edge XAS and μ-XRF analyses (Table S3, Supporting Information). A similar observation was reported by O'Day et al.[43] These results suggest the homogeneous precipitation of realgar or, alternatively, that nanometer-sized Fe sulfides[46] necessary for As(III) reduction (eq 1) were below the analytical detection limits.

The discovery of arsenopyrite in the peat is another surprising finding because this mineral is unstable under the redox conditions encountered in the peat (Figure S8, Supporting Information).[47] An intimate association of ∼10 μm sized arsenopyrite particles with fibrous plant material (Figure 4) hints at an authigenic formation of arsenopyrite, which so far has only been reported for mining-affected sediments in a microcosm study.[16] According to Bostick and Fendorf,[11] the formation of arsenopyrite can proceed by the reaction of As(III) with Fe sulfides:

$$3FeS + H_3AsO_3 \leftrightarrow FeS_2 + FeAsS + Fe(OH)_3 \quad \Delta G^0 = -81.3\ kJ\ mol^{-1} \quad (2)$$

$$7FeS_2 + 2H_3AsO_3 \leftrightarrow 3FeS_4 + 2FeAsS + 2Fe(OH)_3 \quad (3)$$

Here, FeS and FeS_2 represent the troilite polymorph and pyrite, respectively. The reaction products comprise poorly crystalline Fe(III)-(hydr)oxides as well as pyrite (eq 2) and long chain polysulfides like Fe tetrasulfide (eq 3). None of the proposed abiotic formation pathways of arsenopyrite involving Fe sulfides (eqs 2 and 3) are strictly supported by our data, which suggests direct biological controls on its formation. Equation 4, which couples the microbial respiration of organic matter to the reduction of As(III), may present an alternative arsenopyrite formation pathway not involving Fe sulfides but Fe(III)-(hydr)oxides and phyllosilicates like chlorite and biotite as potential Fe^{2+} sources:

$$1/4\ lactate + Fe^{2+} + H_3AsO_3 + H_2S \leftrightarrow FeAsS + 3/4CO_2(g) + 9/4H_2O + 7/4H^+ \quad \Delta G^0 = -95.0\ kJ\ mol^{-1} \quad (4)$$

This reaction would be favored in reducing environments where the generated acidity is effectively buffered by the alkalinity produced during bacterial sulfate reduction. The occurrence of As sulfides in peat samples with "bulk" redox potentials ≥−11 mV generally highlights the presence of strongly reducing microenvironments with variable Fe and S solution concentrations (Figures S8 and S9, Supporting Information).

In the deep peat layer samples, binding of As(III) by about three sulfhydryl groups was the major As sequestration mechanism (Figure 1, Table 1) despite that these samples contained high amounts of pyrite (≤36% of ≤8.3 g Fe kg^{-1}) known to be an effective host for As.[11,12] A maximum of 5 wt%

dx.doi.org/10.1021/es401315e | Environ. Sci. Technol. 2013, 47, 9706−9714

Table 1. Arsenic Speciation Results Based on Linear Combination Fitting of μ-XANES Spectra Collected at Selected Points of Interest (POI) of the B1II, B3II, and B5II Thin Sections

		% of total As (normalized to a sum of 100%)[b]					
sample ID[a]	POI	As(III)−NOM	Realgar	As-Fh	As-Py	fitted sum (%)[c]	NSSR (%)[d]
B3II-31-1	1−10	–	100	–	–	100	0.04
B3II-31-2	1−3	44 (0/44)	–	56 (44/12)	–	104	0.11
	4, 6, 8	–	–	100 (29/71)	–	102	0.08
	5	–	–	100 (44/56)	–	105	0.20
	7	–	84	16 (16/0)	–	104	0.20
B5II-12	1, 2, 4	–	–	–	100 (100/0)	100	0.11
	3	–	–	100 (0/100)	–	100	0.28
B1II-212	1−6	100 (100/0)	–	–	–	100	0.45
B1II-237-1	1	–	–	–	100 (35/65)	103	0.07
	2−6	100 (0/100)	–	–	–	100	0.23
B1II-237-2	1−4	100 (0/100)	–	–	–	100	0.52

[a]The sample ID indicates core label, mean sampling depth of the thin section material in centimeters, and (where applicable) the number of the mapped regions shown in Figures 3 and 4. The POIs in the fine maps are also indicated in Figures 3 and 4. μ-XANES spectra of all POIs are presented in Figure 5. [b]Values in parentheses indicate the fractions of the following reference compounds: As(III)−NOM = tris(phenylthio)arsine (As(III)$(SPhen)_3$)/a mixture of a di- and triglutathione complex of As(III) (As(III)$(GS)_{2.6}(OH)_{0.6}$),[20] As-Fh = As(III)/As(V) sorbed to ferrihydrite, As-Py = arsenopyrite/arsenian pyrite. [c]Fitted sum of all references before normalization. [d]Normalized sum of squared residuals (NSSR (%) = $100 \times \Sigma_i(data_i - fit_i)^2/\Sigma_i data_i^2$).

As in pyrite[48] would correspond to 24−78% of total As in the deep peat layer samples. This suggests that NOM is effectively inhibiting the sorption of As(III) to authigenic pyrite[19] and the substitution of As for S in its structure. The uptake of As by NOM rather than pyrite may be explained by a combination of fast pyrite precipitation, preventing As substitution reactions, and a high thermodynamic stability of the As(III)−NOM complexes. Indeed, the complexation of As(III) by sulfhydryl ligands in aqueous solution is highly favorable. For example, Rey et al.[49] determined a log K of 29.84 (ΔG^0 = −170.2 kJ mol^{-1}) for the reaction of cysteine (Cys = $[C_3H_5NO_2S]^{2-}$) with As(III):

$$3H_2Cys + H_3AsO_3 \leftrightarrow As(HCys)_3 + 3H_2O \quad (5)$$

Our As and S speciation results also indicate that the formation of As(III)−NOM complexes is favored by a high abundance of reduced organic S (Table S4, Supporting Information) and comparatively low As solution concentrations. Surface waters, increasingly depleted in As during infiltration from the near-surface peat layers downward, are likely more and more undersaturated in As with respect to As sulfides, and therefore, As(III) can be effectively sorbed by abundant sulfhydryl groups of NOM. The similar distribution of organic S-coordinated As in peat material featuring different degrees of decomposition (Figure 3e,f vs. Figure 4b) supports a passive sorption mechanism.[37] This reasoning is buttressed by findings showing that a direct uptake of As by plants would result in a localized As enrichment in individual plant tissue (e.g., xylem, cellular vacuoles, or vascular tissue) and does not always involve sulfhydryl groups.[23,50,51] Moreover, As concentrations in various parts of plants collected at our sampling sites are too low to explain the formation of As(III)−NOM complexes by the uptake and intracellular detoxification of As by plants. The above-ground biomass only contained 0.13−11.9 mg As kg^{-1} dry mass (mean: 2.5 mg kg^{-1}, n = 15), whereas root As concentrations, likely biased by high As contents of the peat at sites B3 and B5, ranged from 0.17 to 78.5 mg As kg^{-1} dry mass (mean: 15.6 mg kg^{-1}, n = 8) (Table S7, Supporting Information). Our μ-XAS/XRF study thus provides further evidence for sorptive As(III)−NOM interactions under conditions unfavorable for As sulfide precipitation and therefore emphasizes the need to account for NOM as a sorbent in geochemical equilibrium and transport models used to assess the fate of As in reduced NOM-rich environments.

■ ASSOCIATED CONTENT

Supporting Information

Details on synchrotron measurements, concentrations of major elements in the peat cores, bulk As, Fe, and S speciation results, synchrotron XRD data, light microscopy analyses, elemental correlation plots, tricolor elemental maps, thermodynamic data, E_h−pH diagrams, and As concentrations in plants. This material is available free of charge via the Internet at http://pubs.acs.org.

■ AUTHOR INFORMATION

Corresponding Author

*E-mail: christian.mikutta@env.ethz.ch; phone: +41-44-6336024; fax: +41-44-6331118.

Notes

The authors declare no competing financial interest.

■ ACKNOWLEDGMENTS

We gratefully acknowledge P. Poggiati and M. Sulmoni (Department of Environment, canton Ticino, Switzerland) for the sampling permit, and K. Barmettler, M. Hoffmann, P. Nievergelt, and D. Saile (ETH Zurich) for field and/or laboratory assistance. Micro-XRF/XAS analyses were carried out at the ALS, which is supported by the Director, Office of Science, Office of Basic Energy Sciences, of the U.S. Department of Energy under contract number DE-AC02-05CH11231. We are grateful to S. C. Fakra for her assistance in using beamline 10.3.2. Bulk XAS spectra were measured at the SSRL, a Directorate of SLAC National Accelerator Laboratory and an Office of Science User Facility operated for the US Department of Energy Office of Science by Stanford University. In this regard, we would like to thank M. J. Latimer and E. J. Nelson for their support in using beamline 4-3 and J. Bargar and M. J. Latimer for assistance in using beamline 11-2 and 4-1. Synchrotron XRD measurements were performed at the

powder diffraction station of the MS-Powder beamline at the SLS, Paul Scherrer Institute, Villingen, Switzerland. The support of A. Cervellino (beamline scientist) and P. N. Mandaliev, K. Ehlert, and M. Hoffmann (ETH Zurich) is gratefully acknowledged. This research project was financially supported by the ETH Zurich under grant number 2708-2.

REFERENCES

(1) Rothwell, J. J.; Taylor, K. G.; Chenery, S. R. N.; Cundy, A. B.; Evans, M. G.; Allott, T. E. H. Storage and behavior of As, Sb, Pb, and Cu in ombrotrophic peat bogs under contrasting water table conditions. *Environ. Sci. Technol.* **2010**, *44*, 8497−8502.

(2) La Force, M. J.; Hansel, C. M.; Fendorf, S. Arsenic speciation, seasonal transformations, and co-distribution with iron in a mine waste-influenced palustrine emergent wetland. *Environ. Sci. Technol.* **2000**, *34*, 3937−3943.

(3) Lemly, A. D.; Finger, S. E.; Nelson, M. K. Sources and impacts of irrigation drainwater contaminants in arid wetlands. *Environ. Toxicol. Chem.* **1993**, *12*, 2265−2279.

(4) Dittmar, J.; Voegelin, A.; Roberts, L. C.; Hug, S. J.; Saha, G. C.; Ali, M. A.; Badruzzaman, A. B. M.; Kretzschmar, R. Arsenic accumulation in a paddy field in Bangladesh: Seasonal dynamics and trends over a three-year monitoring period. *Environ. Sci. Technol.* **2010**, *44*, 2925−2931.

(5) Smedley, P. L.; Kinniburgh, D. G. A review of the source, behaviour and distribution of arsenic in natural waters. *Appl. Geochem.* **2002**, *17*, 517−568.

(6) Manning, B. A.; Goldberg, S. Arsenic(III) and arsenic(V) absorption on three California soils. *Soil Sci.* **1997**, *162*, 886−895.

(7) Violante, A.; Pigna, M. Competitive sorption of arsenate and phosphate on different clay minerals and soils. *Soil Sci. Soc. Am. J.* **2002**, *66*, 1788−1796.

(8) Bowell, R. J. Sorption of arsenic by iron-oxides and oxyhydroxides in soils. *Appl. Geochem.* **1994**, *9*, 279−286.

(9) Anawar, H. M.; Akai, J.; Komaki, K.; Terao, H.; Yoshioka, T.; Ishizuka, T.; Safiullah, S.; Kato, K. Geochemical occurrence of arsenic in groundwater of Bangladesh: Sources and mobilization processes. *J. Geochem. Explor.* **2003**, *77*, 109−131.

(10) Masscheleyn, P. H.; Delaune, R. D.; Patrick, W. H. Effect of redox potential and pH on arsenic speciation and solubility in a contaminated soil. *Environ. Sci. Technol.* **1991**, *25*, 1414−1419.

(11) Bostick, B. C.; Fendorf, S. Arsenite sorption on troilite (FeS) and pyrite (FeS_2). *Geochim. Cosmochim. Acta* **2003**, *67*, 909−921.

(12) Lowers, H. A.; Breit, G. N.; Foster, A. L.; Whitney, J.; Yount, J.; Uddin, N.; Muneem, A. Arsenic incorporation into authigenic pyrite, Bengal Basin sediment, Bangladesh. *Geochim. Cosmochim. Acta* **2007**, *71*, 2699−2717.

(13) Dixit, S.; Hering, J. G. Comparison of arsenic(V) and arsenic(III) sorption onto iron oxide minerals: Implications for arsenic mobility. *Environ. Sci. Technol.* **2003**, *37*, 4182−4189.

(14) Root, R. A.; Dixit, S.; Campbell, K. M.; Jew, A. D.; Hering, J. G.; O'Day, P. A. Arsenic sequestration by sorption processes in high-iron sediments. *Geochim. Cosmochim. Acta* **2007**, *71*, 5782−5803.

(15) Moore, J. N.; Ficklin, W. H.; Johns, C. Partitioning of arsenic and metals in reducing sulfidic sediments. *Environ. Sci. Technol.* **1988**, *22*, 432−437.

(16) Rittle, K. A.; Drever, J. I.; Colberg, P. J. S. Precipitation of arsenic during bacterial sulfate reduction. *Geomicrobiol. J.* **1995**, *13*, 1−11.

(17) Buschmann, J.; Kappeler, A.; Lindauer, U.; Kistler, D.; Berg, M.; Sigg, L. Arsenite and arsenate binding to dissolved humic acids: Influence of pH, type of humic acid, and aluminum. *Environ. Sci. Technol.* **2006**, *40*, 6015−6020.

(18) Redman, A. D.; Macalady, D. L.; Ahmann, D. Natural organic matter affects arsenic speciation and sorption onto hematite. *Environ. Sci. Technol.* **2002**, *36*, 2889−2896.

(19) González A., Z. I.; Krachler, M.; Cheburkin, A. K.; Shotyk, W. Spatial distribution of natural enrichments of arsenic, selenium, and uranium in a minerotrophic peatland, Gola di Lago, Canton Ticino, Switzerland. *Environ. Sci. Technol.* **2006**, *40*, 6568−6574.

(20) Langner, P.; Mikutta, C.; Kretzschmar, R. Arsenic sequestration by organic sulphur in peat. *Nat. Geosci.* **2012**, *5*, 66−73.

(21) Zimmer, D.; Kruse, J.; Baum, C.; Borca, C.; Laue, M.; Hause, G.; Meissner, R.; Leinweber, P. Spatial distribution of arsenic and heavy metals in willow roots from a contaminated floodplain soil measured by X-ray fluorescence spectroscopy. *Sci. Total Environ.* **2011**, *409*, 4094−4100.

(22) Frommer, J.; Voegelin, A.; Dittmar, J.; Marcus, M. A.; Kretzschmar, R. Biogeochemical processes and arsenic enrichment around rice roots in paddy soil: Results from micro-focused X-ray spectroscopy. *Eur. J. Soil Sci.* **2011**, *62*, 305−317.

(23) Castillo-Michel, H.; Hernandez-Viezcas, J.; Dokken, K. M.; Marcus, M. A.; Peralta-Videa, J. R.; Gardea-Torresdey, J. L. Localization and speciation of arsenic in soil and desert plant Parkinsonia florida using μ-XRF and μ-XANES. *Environ. Sci. Technol.* **2011**, *45*, 7848−7854.

(24) Strawn, D.; Doner, H.; Zavarin, M.; McHugo, S. Microscale investigation into the geochemistry of arsenic, selenium, and iron in soil developed in pyritic shale materials. *Geoderma* **2002**, *108*, 237−257.

(25) Landrot, G.; Tappero, R.; Webb, S. M.; Sparks, D. L. Arsenic and chromium speciation in an urban contaminated soil. *Chemosphere* **2012**, *88*, 1196−1201.

(26) Prietzel, J.; Botzaki, A.; Tyufekchieva, N.; Brettholle, M.; Thieme, J.; Klysubun, W. Sulfur speciation in soil by S K-edge XANES spectroscopy: Comparison of spectral deconvolution and linear combination fitting. *Environ. Sci. Technol.* **2011**, *45*, 2878−2886.

(27) Griffin, R. A.; Jurinak, J. J. Estimation of activitiy coefficients from electrical conductivity of natural aquatic systems and soil extracts. *Soil Sci.* **1973**, *116*, 26−30.

(28) Delvigne, J. E. *Atlas of micromorphology of mineral alteration and weathering*; Mineralogical Association of Canada: Ottawa, 1998.

(29) Bonazzi, P.; Menchetti, S.; Pratesi, G. The crystal structure of pararealgar, As_4S_4. *Am. Mineral.* **1995**, *80*, 400−403.

(30) Mullen, D. J. E.; Nowacki, W. Refinement of crystal structures of realgar, AsS and orpiment, As_2S_3. *Z. Kristallogr.* **1972**, *136*, 48−65.

(31) Bonazzi, P.; Bindi, L. A crystallographic review of arsenic sulfides: Effects of chemical variations and changes induced by exposure to light. *Z. Kristallogr.* **2008**, *223*, 132−147.

(32) Kutoglu, A. Preparation and crystal-structure of a new isomeric form of As_4S_4. *Z. Anorg. Allg. Chem.* **1976**, *419*, 176−184.

(33) Tuktabiev, M. A.; Popova, S. V.; Brazhkin, V. V.; Lyapin, A. G.; Katayama, Y. Compressibility and polymorphism of α-As_4S_4 realgar under high pressure. *J. Phys.: Condens. Matter* **2009**, *21*, 1−7.

(34) Vairavamurthy, A. Using X-ray absorption to probe sulfur oxidation states in complex molecules. *Spectrochim. Acta, Part A* **1998**, *54*, 2009−2017.

(35) Manceau, A.; Nagy, K. L. Quantitative analysis of sulfur functional groups in natural organic matter by XANES spectroscopy. *Geochim. Cosmochim. Acta* **2012**, *99*, 206−223.

(36) Bolin, T. B. Direct determination of pyrite content in Argonne premium coals by the use of sulfur X-ray near edge absorption spectroscopy (S-XANES). *Energy Fuels* **2010**, *24*, 5479−5482.

(37) Hoffmann, M.; Mikutta, C.; Kretzschmar, R. Bisulfide reaction with natural organic matter enhances arsenite sorption: Insights from X-ray absorption spectroscopy. *Environ. Sci. Technol.* **2012**, *46*, 11788−11797.

(38) Skyllberg, U.; Xia, K.; Bloom, P. R.; Nater, E. A.; Bleam, W. F. Binding of mercury(II) to reduced sulfur in soil organic matter along upland-peat soil transects. *J. Environ. Qual.* **2000**, *29*, 855−865.

(39) Zhao, F. J.; Lehmann, J.; Solomon, D.; Fox, M. A.; McGrath, S. P. Sulphur speciation and turnover in soils: Evidence from sulphur K-edge XANES spectroscopy and isotope dilution studies. *Soil Biol. Biochem.* **2006**, *38*, 1000−1007.

(40) Prietzel, J.; Thieme, J.; Salome, M.; Knicker, H. Sulfur K-edge XANES spectroscopy reveals differences in sulfur speciation of bulk

soils, humic acid, fulvic acid, and particle size separates. *Soil Biol. Biochem.* **2007**, *39*, 877−890.
(41) Prietzel, J.; Tyufekchieva, N.; Eusterhues, K.; Kogel-Knabner, I.; Thieme, J.; Paterson, D.; McNulty, I.; de Jonge, M.; Eichert, D.; Salome, M. Anoxic versus oxic sample pretreatment: Effects on the speciation of sulfur and iron in well-aerated and wetland soils as assessed by X-ray absorption near-edge spectroscopy (XANES). *Geoderma* **2009**, *153*, 318−330.
(42) Xia, K.; Weesner, F.; Bleam, W. F.; Bloom, P. R.; Skyllberg, U. L.; Helmke, P. A. XANES studies of oxidation states of sulfur in aquatic and soil humic substances. *Soil Sci. Soc. Am. J.* **1998**, *62*, 1240−1246.
(43) O'Day, P. A.; Vlassopoulos, D.; Root, R.; Rivera, N. The influence of sulfur and iron on dissolved arsenic concentrations in the shallow subsurface under changing redox conditions. *Proc. Natl. Acad. Sci. U.S.A.* **2004**, *101*, 13703−13708.
(44) Gallegos, T. J.; Han, Y.-S.; Hayes, K. F. Model predictions of realgar precipitation by reaction of As(III) with synthetic mackinawite under anoxic conditions. *Environ. Sci. Technol.* **2008**, *42*, 9338−9343.
(45) Gallegos, T. J.; Hyun, S. P.; Hayes, K. F. Spectroscopic investigation of the uptake of arsenite from solution by synthetic mackinawite. *Environ. Sci. Technol.* **2007**, *41*, 7781−7786.
(46) Wolthers, M.; Van der Gaast, S. J.; Rickard, D. The structure of disordered mackinawite. *Am. Mineral.* **2003**, *88*, 2007−2015.
(47) Craw, D.; Falconer, D.; Youngson, J. H. Environmental arsenopyrite stability and dissolution: Theory, experiment, and field observations. *Chem. Geol.* **2003**, *199*, 71−82.
(48) Savage, K. S.; Tingle, T. N.; O'Day, P. A.; Waychunas, G. A.; Bird, D. K. Arsenic speciation in pyrite and secondary weathering phases, Mother Lode Gold District, Tuolumne County, California. *Appl. Geochem.* **2000**, *15*, 1219−1244.
(49) Rey, N. A.; Howarth, O. W.; Pereira-Maia, E. C. Equilibrium characterization of the As(III)-cysteine and the As(III)-glutathione systems in aqueous solution. *J. Inorg. Biochem.* **2004**, *98*, 1151−1159.
(50) Seyfferth, A. L.; Webb, S. M.; Andrews, J. C.; Fendorf, S. Defining the distribution of arsenic species and plant nutrients in rice (Oryza sativa L.) from the root to the grain. *Geochim. Cosmochim. Acta* **2011**, *75*, 6655−6671.
(51) Pickering, I. J.; Gumaelius, L.; Harris, H. H.; Prince, R. C.; Hirsch, G.; Banks, J. A.; Salt, D. E.; George, G. N. Localizing the biochemical transformations of arsenate in a hyperaccumulating fern. *Environ. Sci. Technol.* **2006**, *40*, 5010−5014.